ACS OMEGA

http://pubs.acs.org/journal/acsodf

Article

Synthesis and Testing of Monoethylene Glycol Carbon Quantum Dots for Inhibition of Hydrates in CO_2 Sequestration

Tinku Saikia,* Jaber Al-Jaberi, and Abdullah Sultan*

Cite This: *ACS Omega* 2021, 6, 15136−15146

Read Online

ACCESS | Metrics & More | Article Recommendations

ABSTRACT: The hydrate formation during the transportation and injection of carbon dioxide in pipelines always leads to the risk of plugging. The development of a cost-efficient CO_2 sequestration method requires efficient hydrate inhibitors. In this research work, the synthesized carbon quantum dots (CQDs) of monoethylene glycol (MEG) were tested with CO_2 hydrates for their hydrate inhibition efficiency. The hydrothermal method was used for the synthesis of CQDs. The synthesized CQDs were characterized using UV light (365 nm), UV−vis absorption, Fourier transform infrared spectroscopy (FTIR), transmission electron microscopy (TEM), and photoluminescence (PL) spectroscopy. MEG CQDs were found to have very good water solubility and fluorescence properties. The MEG CQDs were tested for their CO_2 hydrate inhibition efficiency using the sapphire rocking cell unit. Test results proved that MEG CQDs are much more effective as a CO_2 hydrate inhibitor in comparison to MEG.

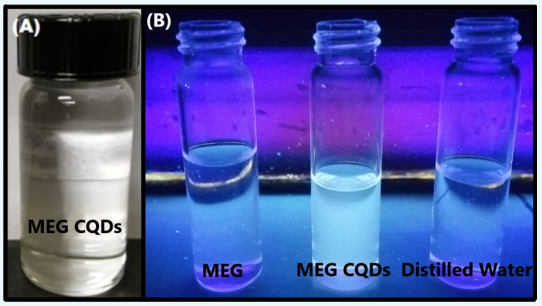

1. INTRODUCTION

Carbon capture for decarbonization and storage (CCS) is one of the most feasible and abating technology for solving the problem of greenhouse gases in the atmosphere and reducing anthropogenic CO_2 emissions.[1] For the decarbonization of the industries and to limit global temperature increase, the upscaling of the CCS technology is very much required. CCS was found to be a proven method for the storage of a large volume of carbon dioxide in underground geological formations. Pilot projects at Sleipner, Snøhvit, In Salah, Weyburn, Boundary Dam, and Quest present successful technical feasibility studies.[2] In the CCS project, a network of the pipeline is used to transport carbon dioxide from the source to the sink. Pipeline transport is an economical way of transporting carbon dioxide in the form of liquid or supercritical/dense-phase liquid.[3] The carbon dioxide coming from power plants was dehydrated to a certain level, whereas even after that, carbon dioxide always contains moisture.[4] For the CCS, the specified water content limit was usually varied between 40 and 500 ppm.[5] Meanwhile, very limited literature is available for supporting these concentration range limits. The occurrence of free water in carbon dioxide resulted in corrosion and hydrate formation. The CCS technology requires a strong emphasis on economic implementation and cost efficiency. Therefore, strict water dehydration limits will add to the cost of CCS projects. The carbon dioxide hydrate formation in the pipelines is a major problem during the transportation and injection phase. This requires special CO_2 hydrate inhibition strategies to solve the problem economically.

On the other hand, carbon dioxide hydrate formation is also a prominent problem in the reservoirs like the giant pre-salt reservoirs found in Brazil, where the carbon dioxide gas volume reaches 80% of the produced gas.[6] This type of reservoir is found in ultradeep waters up to a depth of 1500 m. At such depths, the pressure and temperature conditions were very much suitable for CO_2 hydrate formation. During the gas production and reinjection of CO_2 gas in such reservoirs, the problem of hydrate blockage always exists.

One of the most efficient and economic strategies to reduce the hydrate plugging problem is the use of hydrate inhibitors. The hydrate inhibitors can be broadly classified as thermodynamic hydrate inhibitors (THIs) and kinetic hydrate inhibitors (KHIs). The THIs shift the phase equilibria to higher pressure and lower temperature conditions. The common THIs are ethylene glycol, diethylene glycol, triethylene glycol, ethanol, methanol, and glycerol. The drawbacks associated with THIs are the requirement of higher concentration (30−50% by weight), solvent regeneration requiring high energy demand, the requirement of inhibitor replacement, and the toxic nature of conventional THIs at higher concentrations that proved to be harmful to the environment.[3,7,8] The KHIs inhibit the gas

Received: March 13, 2021
Accepted: May 19, 2021
Published: June 1, 2021

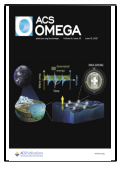

https://doi.org/10.1021/acsomega.1c01355
ACS Omega 2021, 6, 15136−15146

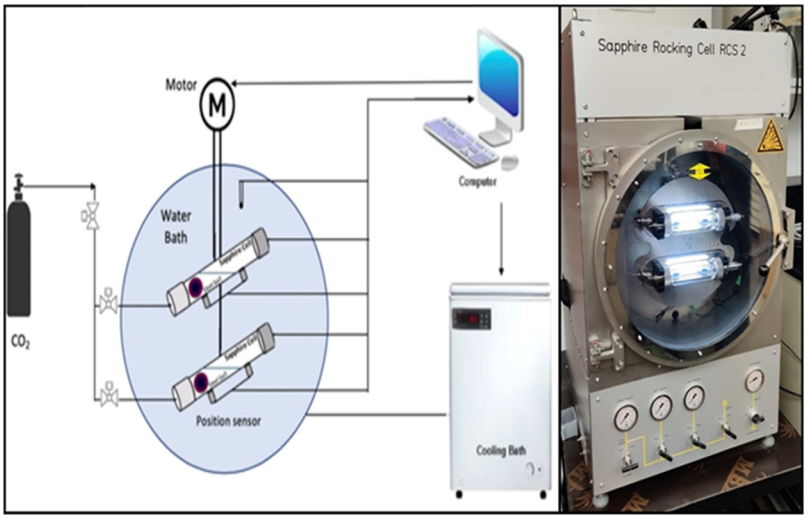

Figure 1. Schematic of the experimental setup for clathrate hydrate induction studies.

hydrate formation by delaying the nucleation stage and retarding the gas hydrate crystal growth at lower concentrations (below 1% by weight).[9−11] The lower concentration requirement of KHIs is a big advantage over THIs, whereas the capability of KHIs for hydrate inhibition is associated with the uncertainties arising from the stochastic nature of hydrate formation and different kinetic factors, and the KHI inhibition effect is time-limited.[3,12] Many researchers present different types of CO_2 gas hydrate inhibitors such as Roosta *et al.* who tested different amino acids (glycine, L-proline, L-serine, L-threonine, L-glutamine, and L-histidine),[13] Sa *et al.* who suggested the use of glycine, L-alanine, and L-valine,[3] and Ramos *et al.* who synthesized three hydrate inhibitors (pentyl L-threonine hydrochloride, nonyl L-threonine hydrochloride, and dodecyl L-threonine hydrochloride).[6] Meanwhile, the search for novel THIs is very much essential for solving the associated problems.[14]

The new THIs should be able to form hydrogen bonds with water molecules, remain stable, and should present environment-friendly characteristics. In this research work, monoethylene glycol (MEG) is selected for modifying and enhancing the inhibition efficiency. Glycols are commonly used as a combined hydrate and corrosion inhibitor in wet gas pipelines (Troll pipeline).[15] Moreover, glycol presents desired properties such as being nonbioaccumulative, degradable, and surface-inactive and having low toxicity.

Carbon quantum dots (CQDs) are at present gaining a lot of interest in all the fields associated with chemistry and chemical engineering because of their characteristics such as excellent water solubility, fluorescence properties, low cost, and chemical stability. The synthesis of (nearly) monodisperse CQDs is possible with the application of hydrothermal or solvothermal methods.[16,17] The CQDs have nanometric size, which is less than 10 nm and can be as smaller as 1 nm. The CQDs have a larger surface area-to-volume ratio.[18] Herein, for the first time, the synthesized monoethylene glycol (MEG) CQDs for the CO_2 hydrate inhibition are tested. In a previous work, the MEG CQD efficiency was tested with tetrahydrofuran hydrates only.[19] To the best of the author's knowledge, this is the first study where it is found that THI CQDs can be effectively used at lower concentrations for CO_2 hydrate inhibition. This modification on the THIs resulted in a new group of hydrate inhibitors, which have the benefits of THIs and can be used at lower concentrations similar to KHIs.

2. EXPERIMENTAL METHODS

2.1. Materials. Monoethylene glycol was purchased from Sigma-Aldrich. The CO_2 gas was used as gas hydrate former (guest molecule in hydrate crystals), and it was obtained from the local gas supplier. The CO_2 gas was provided with a purity of 99.9%.

2.2. Synthesis of THI CQDs. A bottom-up method was used for the synthesis of THI CQDs. The hydrothermal method was used. In this method, the undiluted MEG was subjected to a high temperature of 180 °C for 24 h in a hydrothermal cell. The hydrothermal cell was made up of Teflon-encapsulated stainless steel. The MEG sample was placed inside the cell and sealed using a spring-loaded cap to maintain the high pressure inside the cell developed during heating. After the synthesis process, the CQDs were centrifuged and filtered. The MEG CQDs were stored in a refrigerator below 4 °C for future use.

2.3. Characterization of THI CQDs. After the synthesis of MEG CQDs, its optical properties were tested using 365 nm UV light, UV−vis absorption spectroscopy (USB-2000, Ocean Optics, USA), and photoluminescence spectroscopy (Horiba Fluorolog 3 fluorescence spectrometer). The size and structure analyses of the CQDs were performed using a high-resolution transmission electron microscope (JOEL JEM 2100F). The TENSOR 27 (BRUKER) FTIR spectrometer was used to study the infrared spectrum of absorption or emission of the synthesized MEG CQDs. The comparison of the MEG and MEG CQD FTIR spectra was done to compare their chemical functional groups. The Raman spectra of MEG and MEG CQDs were acquired with a LabRAM HR Evolution Raman spectrometer. The spectrometer was furnished with a HeNe laser (<20 mW). The Raman spectra were obtained at an excitation wavelength of 633 nm.

2.4. Gas Hydrate Inhibition Study. For the CO_2 hydrate inhibition study, the PSL Systemtechnik high-pressure sapphire rocking cell was used; the schematic is shown in Figure 1. The main components of this system are sapphire cells and the computer system for data acquisition and programming. Both the sapphire cells of 20 mL volume include

https://doi.org/10.1021/acsomega.1c01355
ACS Omega 2021, 6, 15136−15146

stainless steel balls to provide the required agitation in the samples during the experiment. The diameter of the stainless steel ball is 10.16 mm and the diameter of the tube is 12.7 mm. The attached motor rocks the cells depending upon the experimental requirements. The time taken by the ball to travel from one sensor to another sensor (installed in both ends) of the sapphire cell is termed ball run time. The ball run time measurement provides information about the agglomeration characteristics of the hydrate crystals. The temperature of the sapphire cells was controlled using an automated temperature control unit consisting of a water bath and chiller. The test started by charging each cell with 10 mL of distilled water−THI solution (i.e., MEG or MEG CQDs were added to distilled water with the needed percentage, which is 10.0% v/v) and placing the cells inside the water bath. Then, the water bath was filled with water, and the cells were flushed four times using CO_2 gas to purge the air molecules from the cells and the flow lines. The pressure was raised in each cell using CO_2 to the desired pressure (i.e., ∼450−500 psi), and the temperature was lowered to 5.0 °C. The rocking frequency was set to 15 times/min. The experiment then started with the pressure maintained in the cells ranging between 430 and 480 psi at 5.0 °C. The cell temperature decreased from 5.0 to 2.0 °C with a prolonged cooling rate of 0.1 °C/h and then from 2.0 to 1.0 °C at a cooling rate of 0.5 °C/h. The temperature was stabilized at every point for 4 h. The point where a sudden pressure drop occurs indicates the point of gas hydrate induction. Meanwhile, sometimes, due to the effect of the gas hydrate inhibitor, the hydrate formation was so slow that the pressure drop is not too prominent; then, the data must be matched with the captured images of the sapphire cell. The condition of the experimental solution in the sapphire cell was photographically captured and saved every 1.0 min in the rocking cell computer system. The gas hydrate inhibition study was repeated to validate the obtained results and every time fresh experimental solution of THIs and distilled water was prepared for testing, to avoid the memory effect.

2.5. Volumetric Gas Uptake Calculation. The number of moles of gas entrapped in the solid hydrate phase at any point of the experiment can be calculated with the help of a real gas equation:

$$\Delta n_t = \left(\frac{PV}{ZRT}\right)_{t=0} - \left(\frac{PV}{ZRT}\right)_t \quad (1)$$

where P is the sapphire cell pressure, V is the gaseous volume, T is the sapphire cell temperature, R is the ideal gas constant, Z is the compressibility factor (the gas compressibility factor was estimated using Pitzer correlations).[20]

In the experimental solution, the CO_2 gas dissolution takes place even before hydrate nucleation and the major portion of the dissolved CO_2 participated in the hydrate crystal formation as a guest molecule. In the gas hydrate crystal, CO_2 is considered as captured and separated from the gas phase.[21]

Equation 1 is valid for calculating the number of moles of gas entrapped in the gas hydrate crystals during the experiment with variation in sapphire cell temperature, as the sapphire rocking cells are a closed system and, during the experiment, the temperature variations lead to consequent pressure variations and both parameters are considered in the equation.

The CO_2 hydrate crystals form a cubic hydrate structure (sI) where each unit cell consists of 46 water molecules and up to 8 CO_2 molecules. These CO_2 molecules occupy both small pentagonal dodecahedral and large tetrakaidecahedral cavities in the hydrate crystal. There are six large cages and two small cages present in the one-unit cell. If all the cages of the hydrate crystals were occupied, then the theoretical hydration number is 5.75, whereas based on CSMGem calculations under equilibrium conditions, the approximate hydration number is considered as 7.03 for the experimental work in this research paper.[21,22]

The water conversion to hydrates (%) can be calculated with the help of the hydration number as follows:

$$\%n_w^t = \frac{7.03 \times \Delta n_t}{n_w^0} \times 100 \quad (2)$$

where n_w^0 is the number of moles of water (initial) in the sapphire rocking cell.

To compare the experiments with different pressure and temperature conditions, the normalized gas uptake value was calculated:[23]

$$g_t = \frac{\Delta n_t}{n_w^0}(\text{mole of gas per mole of water}) \quad (3)$$

Volumetric gas uptake that compares the experiments with different experimental conditions can be calculated using eq 4:

$$vg_t = \frac{\Delta n_t \times 22400}{(n_w^0 - 7.03\Delta n_t)\left(\frac{MW_{H_2O}}{\rho_{H_2O}}\right) + \left(\Delta n_t \times \frac{MW_{hydrate}}{\rho_{hydrate}}\right)} \quad (4)$$

where MW_{H_2O} is the molecular weight of water, ρ_{H_2O} is the density of water, $MW_{hydrate}$ is the molecular weight of hydrate, and $\rho_{hydrate}$ is the density of hydrate.

The volumetric gas uptake is calculated after the induction point of hydrate in the experimental solution to study the effect of the hydrate inhibitor and it represents the hydrate growth. The dissolution of CO_2 gas in the liquid phase before the hydrate crystal induction point was not taken into account because it will not help understand the efficiency of the hydrate inhibitor in restricting the gas uptake in the hydrate crystals.

3. RESULTS AND DISCUSSION

3.1. THI CQD Characterization. The carbon quantum dots were synthesized using the bottom-up method (i.e., hydrothermal method). The synthesized CQDs dispersed in monoethylene glycol were checked under normal light and UV light (365 nm). The MEG CQDs under visible light were transparent with no color. Under UV light, the synthesized MEG CQDs showed strong bluish color fluorescence emission, whereas the MEG and distilled water showed no fluorescence (Figure 2). Many researchers found that this fluorescence is due to the "quantum confinement" effect.[24] It was found that the increase or decrease in energy bandgap size may occur with variation in the size of quantum dots. Emission of large-wavelength photons (redshift) was mainly seen from larger-sized quantum dots due to a decrease in the energy bandgap, whereas smaller-sized quantum dots showed an increase in the energy bandgap and emit short-wavelength light (blueshift).

The carbon nanodots are spherical and they can be grouped as carbon quantum dots (with crystal lattice) and carbon nanoparticles (without crystal lattice).[25] The average interlayer distance of CQDs corresponds to crystalline graphite spacing (002) and the value is generally ca. 0.34 nm.[26] In Figure 3A,B, the synthesized carbon quantum dots of MEG can be seen as

https://doi.org/10.1021/acsomega.1c01355
ACS Omega 2021, 6, 15136−15146

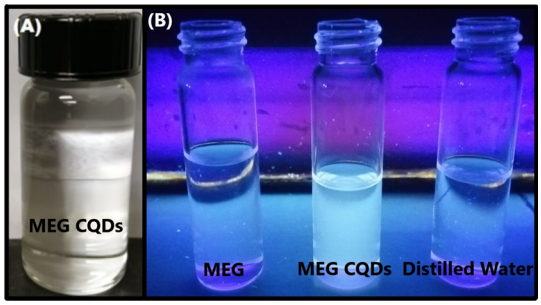

Figure 2. (A) MEG CQDs in visible light; (B) distilled water, MEG, and MEG CQDs under UV light of 365 nm.

uniform in size and spherical; this indicates that the synthesized CQDs are showing monodispersity. In Figure 3B, the lattice fringes can be easily identified within the CQDs, indicating crystalline characteristics. The lattice spacing in the MEG CQDs was found to be 0.104 nm. Usually, the synthesized CQDs from a synthetic molecular carbon source or natural source show the entire amorphous structure or amorphous outer shell with a crystalline core.[27] However, in this work, the hydrothermal method synthesized CQDs that have a complete crystalline structure. The hydrothermal method of synthesis also provides narrower particle size distribution of synthesized CQDs because much needed homogeneous nucleation required to maintain the size was possible due to the use of molecular carbon precursors.[28] The particle size distribution of the MEG CQDs is shown in the inset of Figure 3 with an average particle size of 4.3 nm.

The FTIR spectra of MEG and MEG CQDs are shown in Figure 4. In the figure, different absorption peaks are present. The peak at 3300 cm^{-1} can be attributed to the vibration of the −OH group in the structure. Both peaks at 2935 and 2873 cm^{-1} are attributed to the stretching between the C−H fragment carbon compounds. The stretching of C−C (i.e., the aliphatic carbon compound) is reflected with the peak at 1207 cm^{-1}. No changes were seen in the absorption peaks of CQDs of MEG as compared to the FTIR spectrum of MEG. It confirms that there is no change in functional groups present in MEG due to the hydrothermal synthesis method. Many research works explain that the absence of some peaks in the

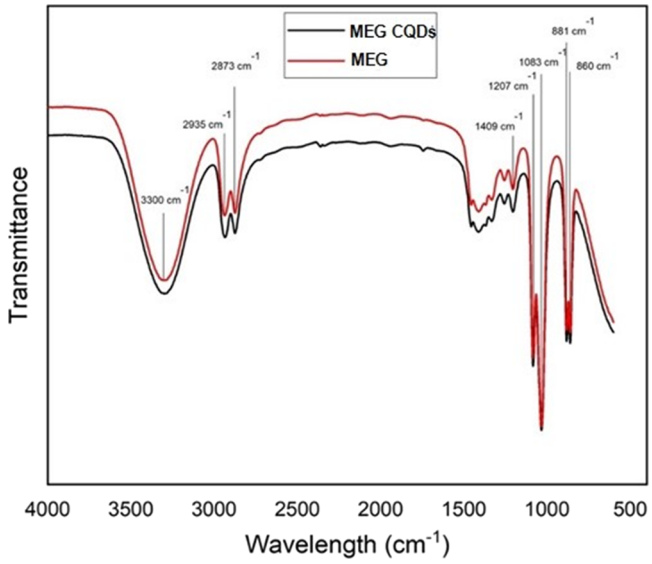

Figure 4. FTIR spectra of MEG and MEG CQDs.

CQD FTIR spectra indicates complete carbonization of the original carbon source. It was said that the presence of functional groups from the initial carbon source indicates insufficient carbonization and may lead to poor photoluminescence.[29] Meanwhile, in this work, the FTIR spectrum of the CQDs after the hydrothermal synthesis process was found to be identical with MEG. The photoluminescence spectrum (Figure 5), as well as the blueshift of CQDs under UV light, seemed to be very good. Moreover, the objective of synthesizing the CQDs of MEG is only to increase its hydrate inhibition performance.

The PL spectrum of the synthesized CQDs is shown in Figure 5. The PL mechanism is still debated, but PL mechanisms involving excitation-independent and excitation-dependent PL are the most accepted ones. The explanation for the excitation-dependent PL was explained as per quantum confinement effect, synergistic models, surface traps, and the heteroatom electronegativity for carbon nanostructures and CQDs.[30−33] Moreover, the probable explanations for excitation-independent PL are the ones associated with the surface state, i.e., shape (hollow interiors) of CQDs and the

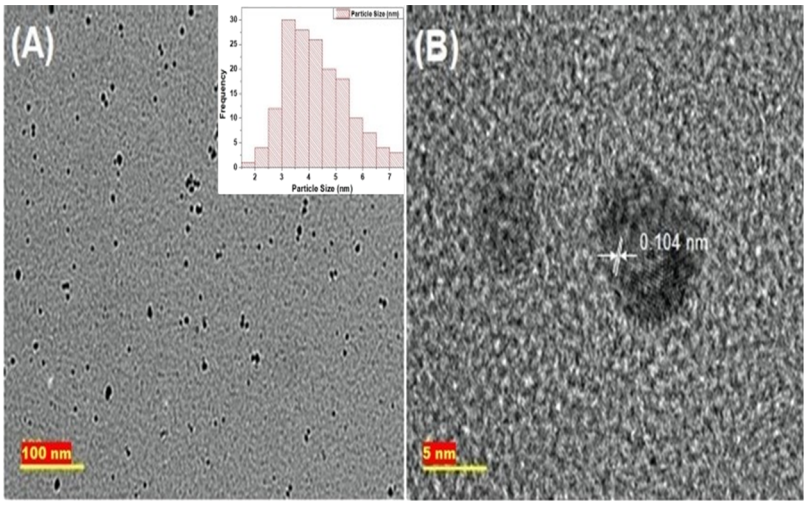

Figure 3. (A, B) HRTEM images of MEG CQDs formed at different scales (100 and 5 nm).

https://doi.org/10.1021/acsomega.1c01355
ACS Omega 2021, 6, 15136−15146

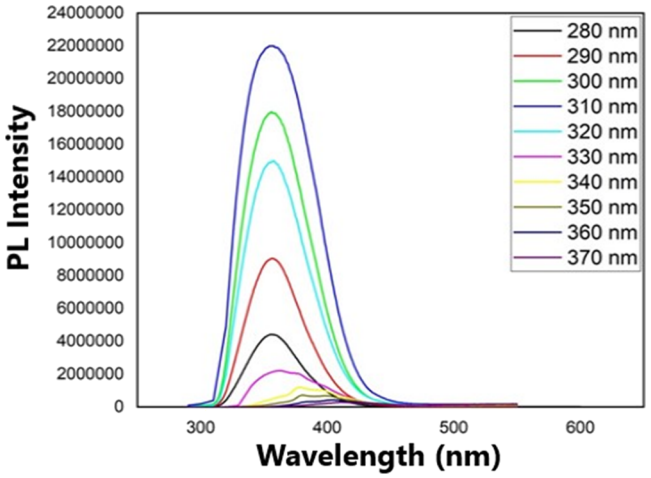

Figure 5. Photoluminescence spectra of one-pot-synthesized MEG CQDs at different excitations.

degree of carbonization.[31] Figure 5 represents the excitation wavelength-dependent PL spectra of synthesized CQDs. The emission intensity changed with increasing excitation wavelength. The figure shows how the intensity emission changes as the excitation wavelength changes from 280 to 370 nm. The highest emission intensity was observed at the excitation wavelength of 310 nm and it is centered at 359 nm.

Figure 6 shows the UV−vis spectrum of the synthesized CQDs. The absorption peak of the CQDs was at 228 nm representing the $\sigma-\sigma^*$ electronic transition of C−C on the MEG CQD surface.

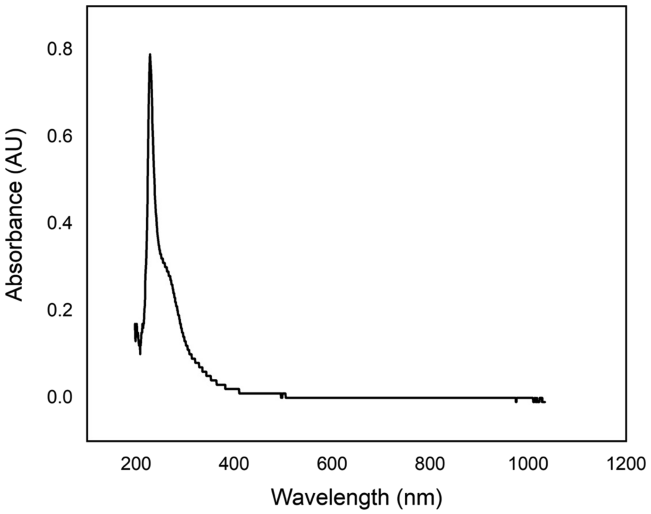

Figure 6. UV−vis absorption of the MEG CQDs in aqueous solution.

Raman spectroscopy has been used to identify the aggregation of CQDs. The smaller size of the CQDs is expected to have higher intensity due to surface-enhanced Raman scattering with surface plasmon resonances. For the aggregates, a slight shift in the Raman bands is anticipated due to phase transition.

The vibrational properties of CQDs of MEG and the MEG pure sample were analyzed by Raman spectroscopy (Figure 7). The fingerprints of CQDs in MEG appeared at 1092, 1468, and 1279 cm^{-1}, which showed an increase in the intensity of 15% when compared to pure MEG solution. No Raman shift due to aggregation of CQDs was observed. Both solutions gave identical ratios as observed for the dominant peaks at 2880 and 2956 cm^{-1} (which is 0.98).

3.2. MEG CQD Hydrate Inhibition Testing. The formation of CO_2 hydrate is a combination of hydrate nucleation and hydrate crystal growth. The CO_2 gas consumption varied in different stages of the hydrate formation. The first stage is the dissolution of CO_2 in water, the second stage is the nucleation of the hydrate crystals, and the third stage is the hydrate crystal growth process. The hydrate crystal nucleation process is a microscopic phenomenon in which tens of thousands of molecules participated.[34] In this nucleation process, hydrate nuclei are formed, which are a small labile cluster made up of water and gas molecules. The hydrate nuclei then grow and disperse in water. These nuclei continuously gather gas in their clusters until the concentration and size reached their critical nuclei required for the hydrate crystal formation. After the nucleation, the hydrate crystal growth is continuous, and it started the agglomeration. For the hydrate crystal growth stage, the mass transfer of the CO_2 gas is very important for hydrate formation. Apart from the mass transfer, the growth kinetics, and the hydrate crystal exothermic growth process, heat transfer from the crystal surface to the solution is also a prominent phenomenon associated with hydrate crystal growth.[35]

In the inhibition study experiments, the CO_2 hydrate formation equilibrium pressure and temperature conditions were maintained. The hydrate inhibition efficiency of MEG and the MEG CQDs (both at 10% v/v concentration) in water under CO_2 hydrate equilibrium conditions was studied (shown in Figures 8−12). MEG has two hydroxyl groups that restrict the water molecules from forming the hydrate crystal cages by making hydrogen bonds with multiple water molecules.[36] The aqueous phase chemical potential of hydrate formation decreases with increasing concentration of MEG in the aqueous phase.[36] This results in shifting of the hydrate equilibrium conditions toward the higher pressure and lower temperature region. The kinetics of hydrate crystal nucleation and formation is dependent on the MEG concentration in the aqueous phase. According to the local structuring mechanism, once the system surpasses the free-energy barrier to hydrate crystal nucleation, the hydrate crystals start to grow. With the increase in the MEG concentration, the affinity of the MEG toward the water molecules increases, which retards the hydrate structure and phase relaxation and hinders the water molecule rearrangement to form hydrates. This will result in a longer induction time and a slower growth rate of hydrate crystals. According to CO_2 hydrate phase equilibria, the CO_2 hydrate crystal stability region starts at approximately 370 psi and 5.95 °C.[37] In all the experiments, the initial temperature and pressure conditions in the sapphire cells were maintained at 5 °C and ∼450−500 psi, respectively. It can be seen in Figure 8 that MEG at 10% v/v in the aqueous solution inhibited the hydrate nucleation up to 4.18 °C approximately. The induction of the hydrate crystals in Figure 8 can be easily identified at 2247 min because of the sudden pressure drop in the sapphire cell. The sudden pressure drop is encircled in the figure. The rate of hydrate crystal formation and hydrate crystal growth was quite rapid as indicated by the rapid pressure drop after the hydrate induction point (Figure 8). The experimental results shown in Figure 9 present the MEG inhibition 2 experiment; the CO_2 hydrate formation took place at 4.85 °C after 2900 min. The hydrate formation is very quick and, in the

https://doi.org/10.1021/acsomega.1c01355
ACS Omega 2021, 6, 15136−15146

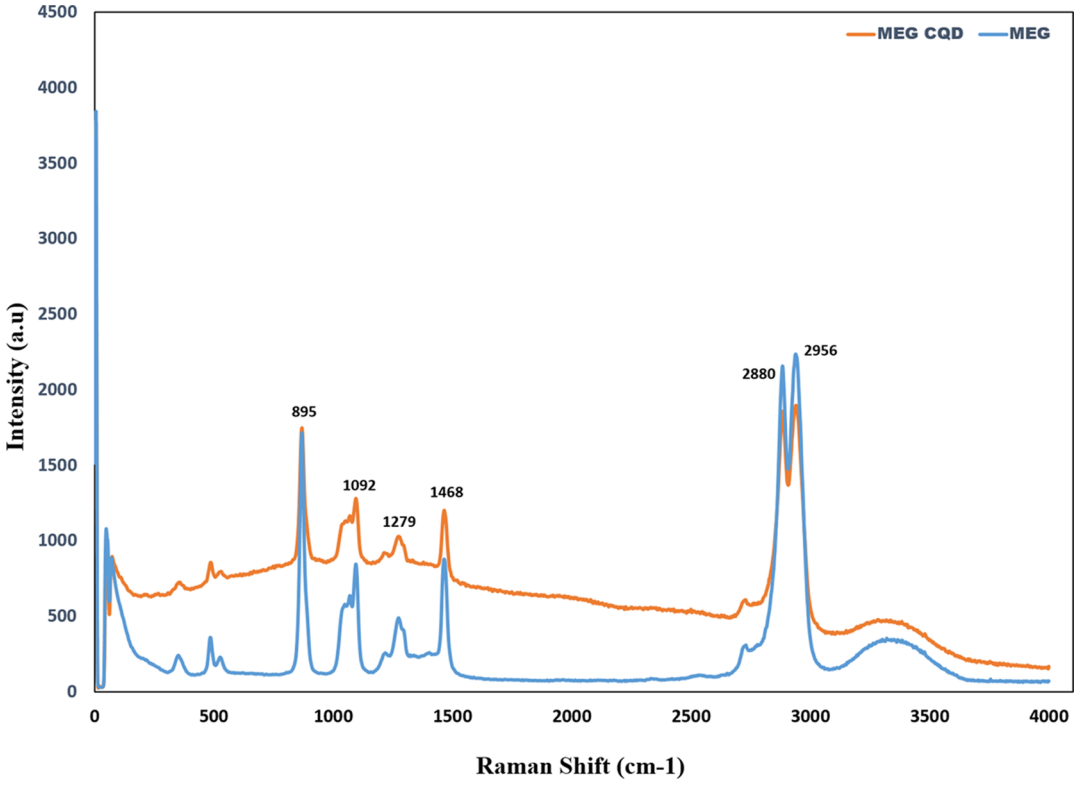

Figure 7. Raman spectra of MEG and MEG CQDs.

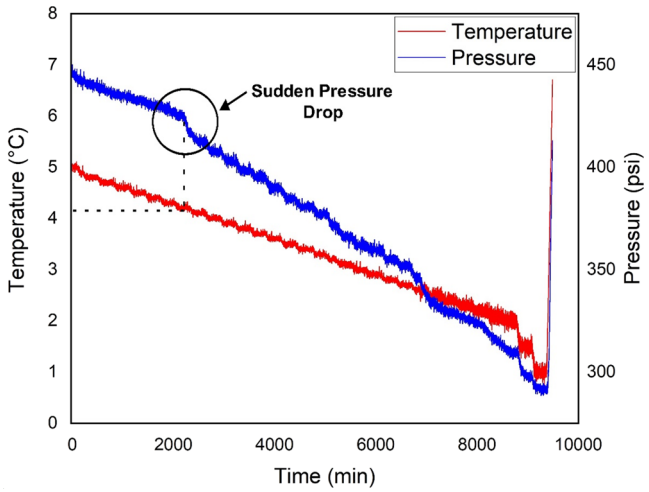

Figure 8. CO_2 gas hydrate inhibition using MEG (MEG inhibition 1).

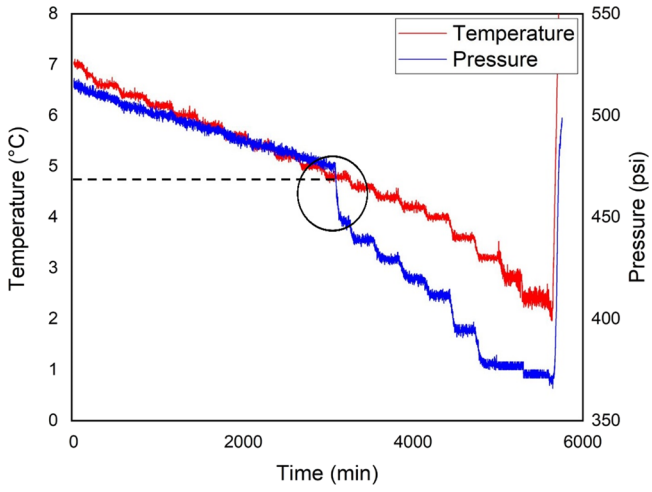

Figure 9. CO_2 gas hydrate inhibition using MEG (MEG inhibition 2).

graph, it can be clearly seen that the pressure drop is very quick, pointing toward the higher rate of hydrate crystal growth. After the induction, the hydrate crystals started to grow and agglomerate with each other, which ultimately blocked the sapphire cell completely as shown in Figure 13A.

The experiment was repeated with the MEG CQDs at the same 10% v/v concentration in the aqueous solution and under the same temperature and pressure conditions. In the experiment, it was seen that the CO_2 hydrate crystal induction was dropped to a temperature of 3.52 °C (Figure 10). The induction time was also considerably increased to 4123 min in comparison to 2247 or 2900 min induction time of hydrate crystals in the MEG solutions. Moreover, the agglomeration of hydrate crystals was prevented by the MEG CQDs, which was verified by the ball run time and visual inspection of the sapphire cell pictures. The gas hydrate crystals in the sapphire cell remain in a slurry form until the end of the cooling cycle, as shown in Figure 13B. The rate of pressure drop after the hydrate induction point is very slow and gradual in comparison to the MEG inhibition experiments. The experiment was repeated another two times (MEG CQD inhibition 2 and 3). The experimental results of the MEG CQD inhibition 2 and 3 experiments are shown in Figures 11 and 12, respectively. In these figures, it was not possible to identify the sudden pressure drop point, but visually, the formation of CO_2 hydrates in the cell was identified. This absence of the sudden pressure drop point is because the CO_2 hydrate nucleation and growth were retarded considerably by the MEG CQDs in the

https://doi.org/10.1021/acsomega.1c01355
ACS Omega 2021, 6, 15136−15146

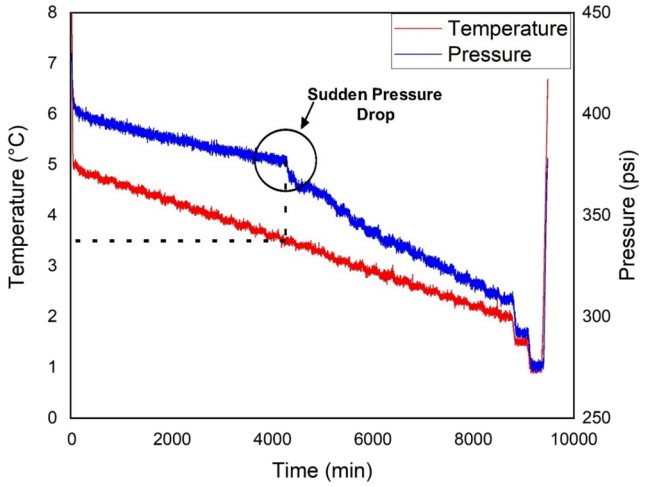

Figure 10. CO_2 gas hydrate inhibition using MEG CQDs (MEG CQD inhibition 1).

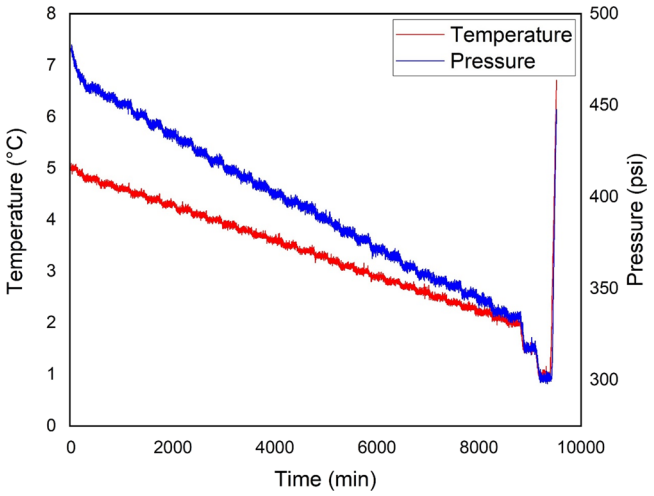

Figure 11. CO_2 gas hydrate inhibition using MEG CQDs (MEG CQD inhibition 2).

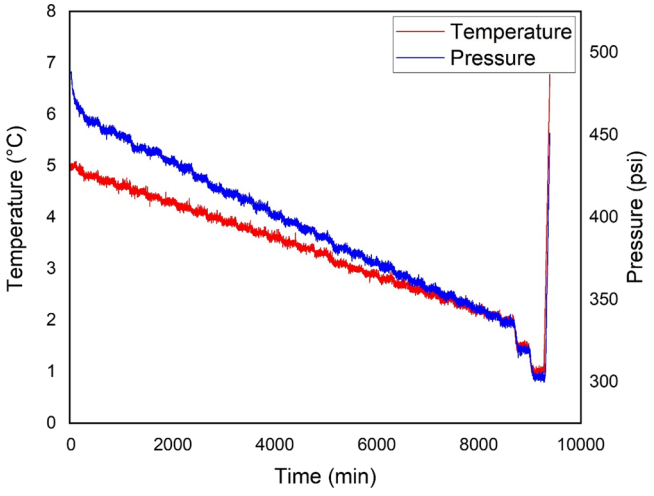

Figure 12. CO_2 gas hydrate inhibition using MEG CQDs (MEG CQD inhibition 3).

sapphire cell. The CO_2 hydrate crystal agglomeration was not seen in the sapphire cell until the end of the experiment.

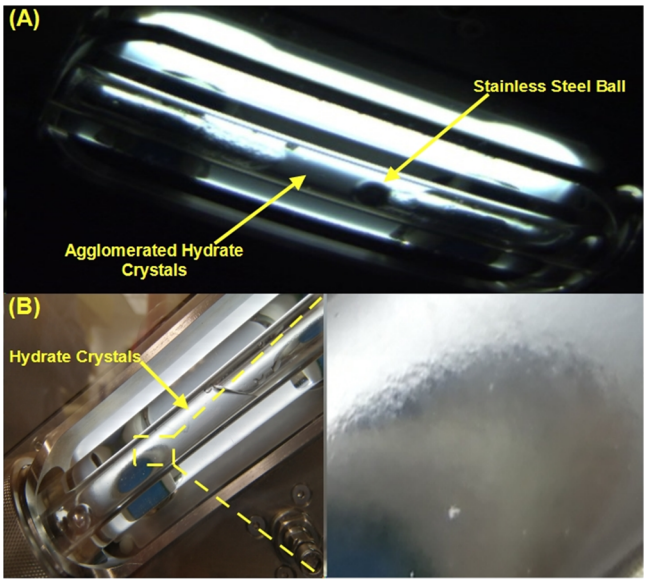

Figure 13. Gas hydrate formation. (A) Agglomerated hydrate crystals in the water–MEG solution and (B) hydrate slurry in the water–MEG CQD solution.

Visually, with the help of sapphire cell pictures as well as taking partial reference to the ball run time, the hydrate induction point was identified in the experiments (MEG CQD inhibition 2 and 3). The CO_2 hydrate crystal induction in the MEG CQD inhibition 2 experiment was found to be at ~3.3 °C with an induction time of ~5100 min. Similarly in the MEG CQD inhibition 3 experiment, the CO_2 hydrate crystal induction was found at ~3.4 °C and an induction time of ~4800 min (Table 1). For the generalized comparison, the mean values of the

Table 1. CO_2 Hydrate Induction Time and Temperature

Sl. no.	experiment	CO_2 hydrate induction temperature (°C)	CO_2 hydrate induction time (min)
1	MEG inhibition (1)	4.18	2247
2	MEG inhibition (2)	4.85	2900
3	MEG CQD inhibition (1)	3.52	4123
4	MEG CQD inhibition (2)	3.3[a]	5100[a]
5	MEG CQD inhibition (3)	3.4[a]	4800[a]

[a]Time and temperature data noted visually and with partial reference to ball run time.

CO_2 hydrate induction temperature and induction time were compared, and it was found that the mean hydrate induction temperature for the MEG inhibition experiment is ~4.5 °C and the hydrate induction time is ~2573 min. The mean values for the MEG CQD inhibition experiment are ~3.4 °C and ~4674 min.

Comparing the CO_2 gas uptake volume in the experimental solution with MEG and MEG CQDs, it can be understood clearly how efficiently an additive is restricting the hydrate crystal growth. The CO_2 gas uptake volume was calculated after the hydrate crystal induction in the solution. The dissolution of the CO_2 gas in the liquid phase before the hydrate crystal induction was not considered. In Figure 14, the

https://doi.org/10.1021/acsomega.1c01355
ACS Omega 2021, 6, 15136−15146

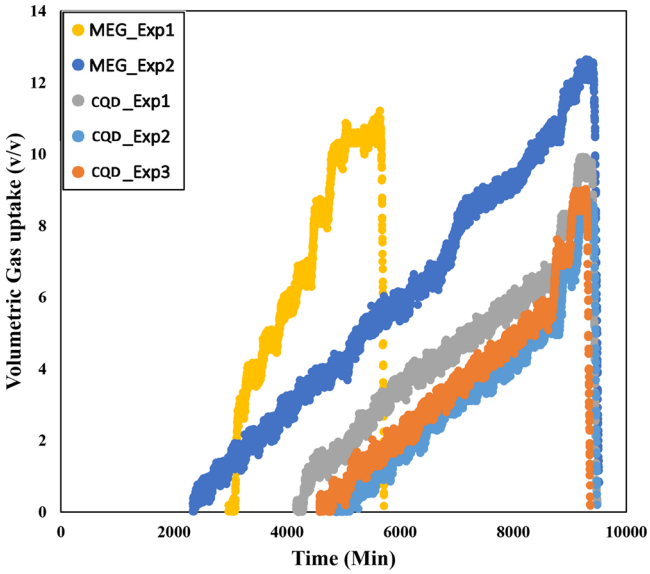

Figure 14. Comparison of volumetric gas uptake in different experiments.

volumetric gas uptake in different experiments to time can be seen. The hydrate crystal induction point in every experiment was the point of origin of CO_2 gas entrapment in the hydrate crystals. The volumetric gas uptake curve in MEG inhibition 1 is steep and the total gas uptake value was found to be 11.21 v/v (Table 2). A similar trend of the steep volumetric gas uptake

Table 2. Total Volumetric Gas Uptake

Sl. no.	experiment	total volumetric gas uptake (v/v)
1	MEG inhibition (1)	11.21
2	MEG inhibition (2)	12.64
3	MEG CQD inhibition (1)	9.92
4	MEG CQD inhibition (2)	8.68
5	MEG CQD inhibition (3)	9.02

curve was seen in the MEG inhibition 2 experiment and the total gas uptake value reached 12.64 v/v. The desired characteristic of the hydrate inhibitor includes an increase in induction time as well as retardation of the hydrate crystal growth. The volumetric gas uptake in the experimental solutions with MEG CQDs is not as steep as in the experimental solution with MEG. The total volumetric gas uptake values were reduced to 9.92, 8.68, and 9.02 v/v for MEG CQD inhibition 1, MEG CQD inhibition 2, and MEG CQD inhibition 3, respectively. This proved that the MEG CQDs are more efficient in comparison to MEG to restrict the hydrate crystal growth.

To statistically compare the MEG and MEG CQD antiagglomeration characteristics, the stainless steel ball run times were compared. The run time measurement provides clear information about the pumpability of the dispersed hydrate crystal solution.[38] It also referenced the intrinsic viscosity changes in the multiphase hydrate crystal slurry. The longer ball running time indicates the increase in viscosity of the slurry in the rocking cell. This increase in viscosity is due to the rapid formation and growth of the hydrate crystals in the solution. Finally, the agglomeration of the hydrate crystals increases the ball run time to very high values.

The change in ball run time during the MEG inhibition 1 experiment is shown in Figure 15. The ball run time plot had

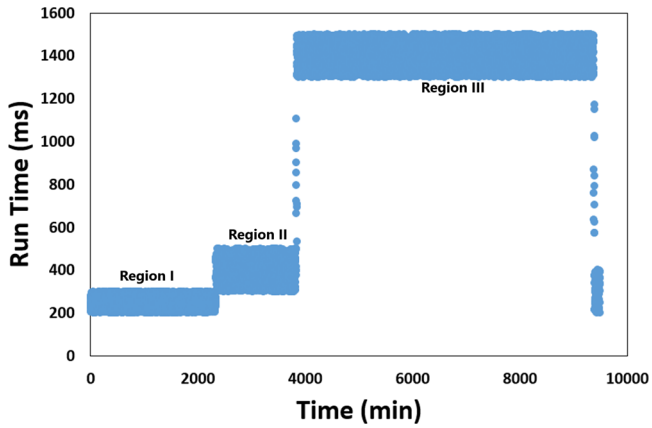

Figure 15. Ball run time during MEG inhibition 1.

three distinct regions and they were named region I, region II, and region III. Region I represents the state of the experimental solution before the induction of hydrate crystals in the sapphire cell. The run time is between 200 and 300 ms. The change in ball run time at around 2338 min indicates the induction of hydrate crystals in the experimental solution, and this was designated as region II. The run time was increased to 500 ms and maintained in between 300 and 500 ms. After approximately 3828 min, another increase in ball run time was observed; the ball run time was increased to 1500 ms, indicating further growth of hydrate crystals in the experimental solution and partial agglomeration (confirmed visually). This region was designated as region III. The partial agglomeration of hydrate crystals was visible, whereas a complete hydrate block was not seen until the end of the experiment.

Similar behavior was seen in the MEG inhibition 2 experiment; in region I, the run time was maintained in between 200 and 300 ms (Figure 16). Approximately after 2968 min, the ball run time was increased to 500 ms in region II. In region III, the ball run time was increased to 1500 ms. But in this experiment, the hydrate crystals agglomerated and formed a hydrate block at the middle portion of the sapphire

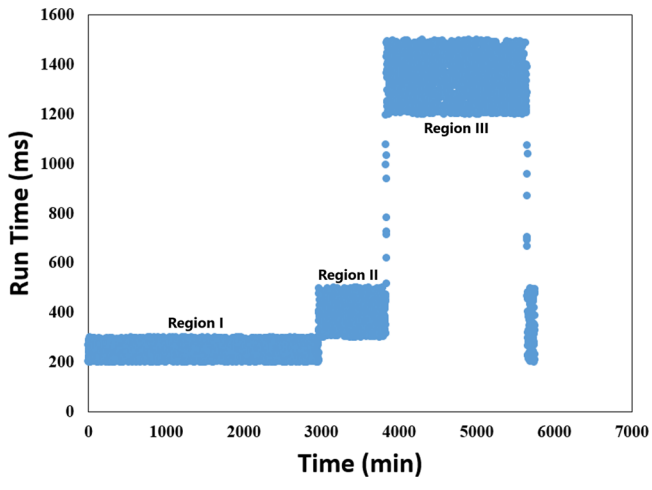

Figure 16. Ball run time during MEG inhibition 2.

https://doi.org/10.1021/acsomega.1c01355
ACS Omega 2021, 6, 15136−15146

cell, as shown in Figure 13A, and after the formation of the hydrate block, the experiment was stopped.

In the MEG CQD inhibition 1 experiment, similar to MEG inhibition 1 and 2 experiments, 200−300 ms ball run time was maintained in region I. But in region II and region III, the increase in the ball run time was limited to 400 and 600 ms, respectively (Figure 17). This decrease in ball run time for

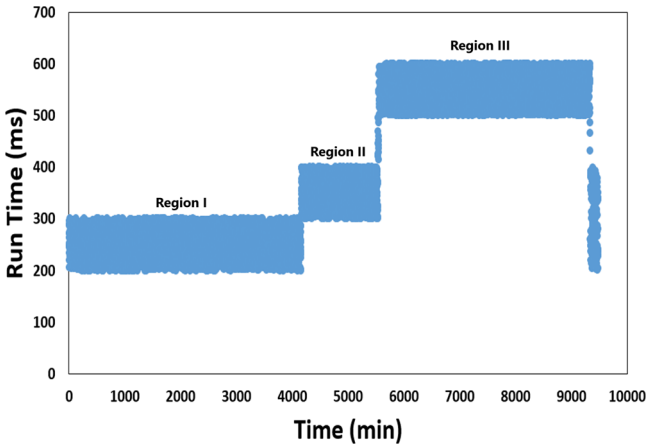

Figure 17. Ball run time during MEG CQD inhibition 1.

MEG inhibition 1 and 2 experiments represents the retarded growth of hydrate crystals in the experimental solution and also the antiagglomerant characteristics of the MEG CQD. The same result was verified visually as the hydrate crystals remain in the slurry form shown in Figure 13B. Similar behavior was seen in MEG CQD inhibition 2 and 3 experiments shown in Figures 18 and 19.

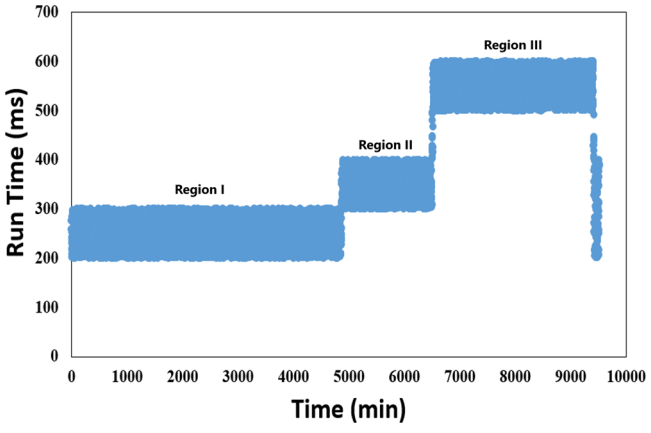

Figure 18. Ball run time during MEG CQD inhibition 2.

Therefore, it can be said that MEG CQDs provide multiple benefits as they decrease the gas hydrate induction temperature, increase the induction time, decrease the volumetric gas uptake, and provide excellent antiagglomeration characteristics. This indicates that a considerably lower concentration of MEG CQDs in comparison to MEG can shift the hydrate equilibrium conditions toward higher pressure and lower temperature. This has a positive effect on economic and environmental issues associated with CO_2 hydrate inhibition.

The enhanced performance of the CQDs may be attributed to the increase in the surface area of the MEG CQDs or maybe lower molecular weight. As we know, the hydrate inhibition

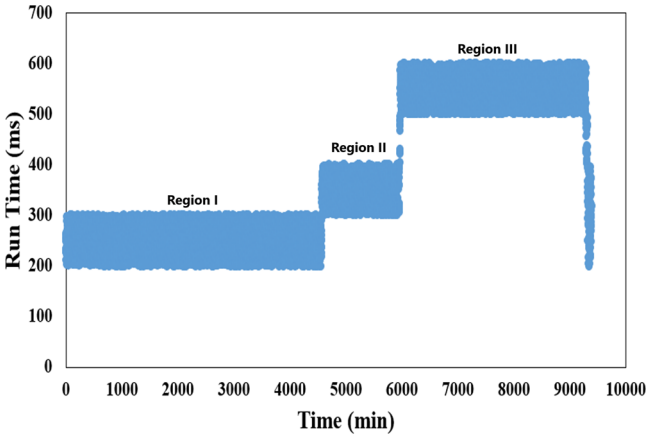

Figure 19. Ball run time during MEG CQD inhibition 3.

performance of the additives with lower molecular weight is better than the higher molecular weight additives.[39] Also, the CQDs have a larger surface area-to-volume ratio.[19,40] A further elaborate study is required to understand the mechanism/properties behind the increased inhibition performance of CQDs.

4. CONCLUSIONS

This research work is the first account of the testing of MEG CQD hydrate inhibition performance with CO_2 hydrate. To commercialize the CO_2 sequestration technology, it is required to make all the aspects of this technology economical. The modification of conventionally available THIs and increasing their hydrate inhibition efficiency are a step toward solving the problems associated with the CO_2 sequestration technology and making them economical for commercialization. The following conclusion can be made from this research study:

1. The hydrothermal treatment method was found to be effective in the preparation of MEG CQDs.
2. All the CQD characterization studies indicated the formation of MEG CQDs with an average particle size of 4.3 nm.
3. During the CO_2 hydrate inhibition experiment, MEG was able to inhibit hydrate formation until 2247 min and the induction of hydrate was seen at 4.18 °C. In the repeat experiment, the hydrate induction was seen after 2900 min at 4.85 °C.
4. The MEG CQD outperformed MEG and inhibits the hydrate formation until 4123 min in the first experiment; the hydrate induction took place at 3.52 °C. In the repeat experiment, the MEG CQD successfully inhibited the hydrate induction until 5100 and 4800 min; the hydrate induction was seen at 3.3 and 3.4 °C, respectively.
5. Out of the three experiments performed with MEG CQDs, two experiments did not show any sudden decrease in pressure, which is considered as a hydrate induction point in the experiments. It is because the MEG CQDs inhibited the hydrate crystal induction and restricted the hydrate crystal growth very efficiently.
6. In the MEG hydrate inhibition experiment, the hydrate crystals showed agglomeration and blocked the sapphire cell. MEG cannot prevent hydrate crystal agglomeration after hydrate induction, which is characteristic of the THIs.

https://doi.org/10.1021/acsomega.1c01355
ACS Omega 2021, 6, 15136−15146

7. The MEG CQDs very efficiently prevented the hydrate crystal agglomeration in all the experiments. The MEG CQDs not only performed better in terms of hydrate inhibition but also presented efficient hydrate agglomeration characteristics.

Finally, it can be concluded that CQDs of different THIs can be used effectively at lower concentrations to prevent CO_2 hydrate formation at any particular temperature and pressure range in comparison to conventional THIs. This will positively impact the usage of THIs (CQDs) in industry since they decrease the cost and improve the performance.

AUTHOR INFORMATION

Corresponding Authors

Tinku Saikia − *Department of Petroleum Engineering, King Fahd University of Petroleum & Minerals, Dhahran 31261, Saudi Arabia;* orcid.org/0000-0001-7230-6074; Phone: +966 (013) 860-1793; Email: tinku.saikia@kfupm.edu.sa; Fax: +966 (013) 860-4447

Abdullah Sultan − *Department of Petroleum Engineering, King Fahd University of Petroleum & Minerals, Dhahran 31261, Saudi Arabia;* orcid.org/0000-0001-9617-4678; Phone: +966 (013) 860-2728/2586; Email: sultanas@kfupm.edu.sa; Fax: +966 (013) 860-4447

Author

Jaber Al-Jaberi − *Department of Petroleum Engineering, King Fahd University of Petroleum & Minerals, Dhahran 31261, Saudi Arabia*

Complete contact information is available at: https://pubs.acs.org/10.1021/acsomega.1c01355

Notes

The authors declare no competing financial interest.

ACKNOWLEDGMENTS

The authors would like to acknowledge the King Fahd University of Petroleum & Minerals for providing necessary laboratory facilities. The authors extend their appreciation to the outstanding support from Mr. Jafar Sadeq Al Hamad from CPG, KFUPM, and Dr. Safyan Akram Khan and Dr. Shahid Ali from CENT, KFUPM.

REFERENCES

(1) Leung, D. Y. C.; Caramanna, G.; Maroto-Valer, M. M. An Overview of Current Status of Carbon Dioxide Capture and Storage Technologies. *Renewable and Sustainable Energy Rev.* **2014**, *39*, 426−443.

(2) Uilhoorn, F. E. Evaluating the Risk of Hydrate Formation in CO2 Pipelines under Transient Operation. *Int. J. Greenh. Gas Control* **2013**, *14*, 177−182.

(3) Sa, J. H.; Lee, B. R.; Park, D. H.; Han, K.; Chun, H. D.; Lee, K. H. Amino Acids as Natural Inhibitors for Hydrate Formation in CO2 Sequestration. *Environ. Sci. Technol.* **2011**, *45*, 5885−5891.

(4) Buit, L.; Ahmad, M.; Mallon, W.; Hage, F. CO2 EuroPipe Study of the Occurrence of Free Water in Dense Phase CO2 Transport. *Energy Procedia* **2011**, *4*, 3056−3062.

(5) de Visser, E.; Hendriks, C.; Barrio, M.; Mølnvik, M. J.; de Koeijer, G.; Liljemark, S.; Le Gallo, Y. Dynamis CO2 Quality Recommendations. *Int. J. Greenh. Gas Control* **2008**, *2*, 478−484.

(6) da Silva Ramos, A.; Pires, J. P.; Medina Ketzer, J. M.; Espíndola de Araújo, G.; Lourega, R. V. Synthesis of New CO2 Hydrate Inhibitors. *J. Nat. Gas Sci. Eng.* **2020**, *75*, 103166.

(7) Saikia, T.; Mahto, V. Experimental Investigations of Clathrate Hydrate Inhibition in Water Based Drilling Fluid Using Green Inhibitor. *J. Pet. Sci. Eng.* **2016**, *147*, 647−653.

(8) Saikia, T.; Mahto, V. Evaluation of 1-Decyl-3-Methylimidazolium Tetrafluoroborate as Clathrate Hydrate Crystal Inhibitor in Drilling Fluid. *J. Nat. Gas Sci. Eng.* **2016**, *36*, 906−915.

(9) Saikia, T.; Mahto, V. Evaluation of Soy Lecithin as Eco-Friendly Biosurfactant Clathrate Hydrate Antiagglomerant Additive. *J. Surfactants Deterg.* **2018**, *21*, 101−111.

(10) Saikia, T.; Mahto, V. Experimental Investigations and Optimizations of Rheological Behavior of Drilling Fluids Using RSM and CCD for Gas Hydrate-Bearing Formation. *Arab. J. Sci. Eng.* **2018**, *43*, 6541−6554.

(11) Kelland, M. A.; Kvæstad, A. H.; Astad, E. L. Tetrahydrofuran Hydrate Crystal Growth Inhibition by Trialkylamine Oxides and Synergism with the Gas Kinetic Hydrate Inhibitor Poly(N-Vinyl Caprolactam). *Energy Fuels* **2012**, *26*, 4454−4464.

(12) Bai, Y.; Bai, Q. *Subsea Engineering Handbook*, 2nd ed.; Gulf Professional Publishing, 2018; pp. 1−968. DOI: 10.1016/C2016-0-03767-1.

(13) Roosta, H.; Dashti, A.; Mazloumi, S. H.; Varaminian, F. Inhibition Properties of New Amino Acids for Prevention of Hydrate Formation in Carbon Dioxide-Water System: Experimental and Modeling Investigations. *J. Mol. Liq.* **2016**, *215*, 656−663.

(14) Xu, Y.; Yang, M.; Yang, X. Chitosan as Green Kinetic Inhibitors for Gas Hydrate Formation. *J. Nat. Gas Chem.* **2010**, *19*, 431−435.

(15) Gulbrandsen, E.; Morard, J. H. *Why Does Glycol Inhibit CO2 Corrosion? In NACE - International Corrosion Conference Series*. San Diego, California, 1998.

(16) Chen, B. B.; Liu, Z. X.; Deng, W. C.; Zhan, L.; Liu, M. L.; Huang, C. Z. A Large-Scale Synthesis of Photoluminescent Carbon Quantum Dots: A Self-Exothermic Reaction Driving the Formation of the Nanocrystalline Core at Room Temperature. *Green Chem.* **2016**, *18*, 5127−5132.

(17) Qu, D.; Zheng, M.; Du, P.; Zhou, Y.; Zhang, L.; Li, D.; Tan, H.; Zhao, Z.; Xie, Z.; Sun, Z. Highly Luminescent S, N Co-Doped Graphene Quantum Dots with Broad Visible Absorption Bands for Visible Light Photocatalysts. *Nanoscale* **2013**, *5*, 12272−12277.

(18) Ng, S. M. Carbon Dots as Optical Nanoprobes for Biosensors. *Nanobiosensors for Biomolecular Targeting.* **2019**, 269−300.

(19) Saikia, T.; Mahto, V.; Kumar, A. Quantum Dots: A New Approach in Thermodynamic Inhibitor for the Drilling of Gas Hydrate Bearing Formation. *J. Ind. Eng. Chem.* **2017**, *52*, 89−98.

(20) Smith, J. M. Introduction to Chemical Engineering Thermodynamics. *J. Chem. Educ.* **1950**, *27*, 584.

(21) Sloan, E. D.; Koh, C. A. *Clathrate Hydrates of Natural Gases*, Thrid Edition; CRC Press, 2007, DOI: 10.1201/9781420008494.

(22) Khandelwal, H.; Qureshi, M. F.; Zheng, J.; Venkataraman, P.; Barckholtz, T. A.; Mhadeshwar, A. B.; Linga, P. Effect of L -Tryptophan in Promoting the Kinetics of Carbon Dioxide Hydrate Formation. *Energy Fuels* **2021**, *35*, 649−658.

(23) Bhattacharjee, G.; Goh, M. N.; Arumuganainar, S. E. K.; Zhang, Y.; Linga, P. Ultra-Rapid Uptake and the Highly Stable Storage of Methane as Combustible Ice. *Energy Environ. Sci.* **2020**, *13*, 4946−4961.

(24) Zuo, J.; Jiang, T.; Zhao, X.; Xiong, X.; Xiao, S.; Zhu, Z. Preparation and Application of Fluorescent Carbon Dots. *J. Nanomater.* **2015**, 1.

(25) Nie, H.; Li, M.; Li, Q.; Liang, S.; Tan, Y.; Sheng, L.; Shi, W.; Zhang, S. X. A. Carbon Dots with Continuously Tunable Full-Color Emission and Their Application in Ratiometric PH Sensing. *Chem. Mater.* **2014**, *26*, 3104−3112.

(26) Zhu, S.; Song, Y.; Zhao, X.; Shao, J.; Zhang, J.; Yang, B. The Photoluminescence Mechanism in Carbon Dots (Graphene Quantum Dots, Carbon Nanodots, and Polymer Dots): Current State and Future Perspective. *Nano Res.* **2015**, *8*, 355−381.

(27) Dager, A.; Uchida, T.; Maekawa, T.; Tachibana, M. Synthesis and Characterization of Mono-Disperse Carbon Quantum Dots from

Fennel Seeds: Photoluminescence Analysis Using Machine Learning. *Sci. Rep.* **2019**, *9*, 14004.
(28) Parvin, N.; Mandal, T. K. Synthesis of a Highly Fluorescence Nitrogen-Doped Carbon Quantum Dots Bioimaging Probe and Its in Vivo Clearance and Printing Applications. *RSC Adv.* **2016**, *6*, 18134−18140.
(29) Tuerhong, M.; Xu, Y.; Yin, X. B. Review on Carbon Dots and Their Applications. *Chin. J. Anal. Chem.* **2017**, *45*, 139−150.
(30) Suzuki, K.; Malfatti, L.; Takahashi, M.; Carboni, D.; Messina, F.; Tokudome, Y.; Takemoto, M.; Innocenzi, P. Design of Carbon Dots Photoluminescence through Organo-Functional Silane Grafting for Solid-State Emitting Devices. *Sci. Rep.* **2017**, *7*, 5469.
(31) Gan, Z.; Xu, H.; Hao, Y. Mechanism for Excitation-Dependent Photoluminescence from Graphene Quantum Dots and Other Graphene Oxide Derivates: Consensus, Debates and Challenges. *Nanoscale* **2016**, *8*, 7794−7807.
(32) Dong, Y.; Wan, L.; Cai, J.; Fang, Q.; Chi, Y.; Chen, G. Natural Carbon-Based Dots from Humic Substances. *Sci. Rep.* **2015**, *5*, 10037.
(33) Liu, X.; Pang, J.; Xu, F.; Zhang, X. Simple Approach to Synthesize Amino-Functionalized Carbon Dots by Carbonization of Chitosan. *Sci. Rep.* **2016**, *6*, 31100.
(34) Mullin, T. *The nature of chaos*, 1st ed.; Clarendon Press, Oxford Science Publications, 1993.
(35) Sun, Q.; Kang, Y. T. Review on CO2 Hydrate Formation/Dissociation and Its Cold Energy Application. *Renewable Sustainable Energy Rev.* **2016**, *62*, 478−494.
(36) Cha, M.; Shin, K.; Kim, J.; Chang, D.; Seo, Y.; Lee, H.; Kang, S. P. Thermodynamic and Kinetic Hydrate Inhibition Performance of Aqueous Ethylene Glycol Solutions for Natural Gas. *Chem. Eng. Sci.* **2013**, *99*, 184−190.
(37) Fan, S. S.; Guo, T. M. Hydrate Formation of CO2-Rich Binary and Quaternary Gas Mixtures in Aqueous Sodium Chloride Solutions. *J. Chem. Eng. Data* **1999**, *44*, 829−832.
(38) Chua, P. C.; Kelland, M. A. Study of the Gas Hydrate Antiagglomerant Performance of a Series of Mono- and Bis-Amine Oxides: Dual Antiagglomerant and Kinetic Hydrate Inhibition Behavior. *Energy Fuels* **2018**, *32*, 1674−1684.
(39) Brustad, S.; Løken, K. P.; Waalmann, J. G. Hydrate Prevention Using MEG Instead of MeOH: Impact of Experience from Major Norwegian Developments on Technology Selection for Injection and Recovery of MEG. In *Proceedings of the Annual Offshore Technology Conference*. 2005. DOI: 10.4043/17355-ms.
(40) Lu, H.; Huang, Z.; Martinez, M. S.; Johnson, J. C.; Luther, J. M.; Beard, M. C. Transforming Energy Using Quantum Dots. *Energy Environ. Sci.* **2020**, *13*, 1347−1376.

https://doi.org/10.1021/acsomega.1c01355
ACS Omega 2021, 6, 15136−15146